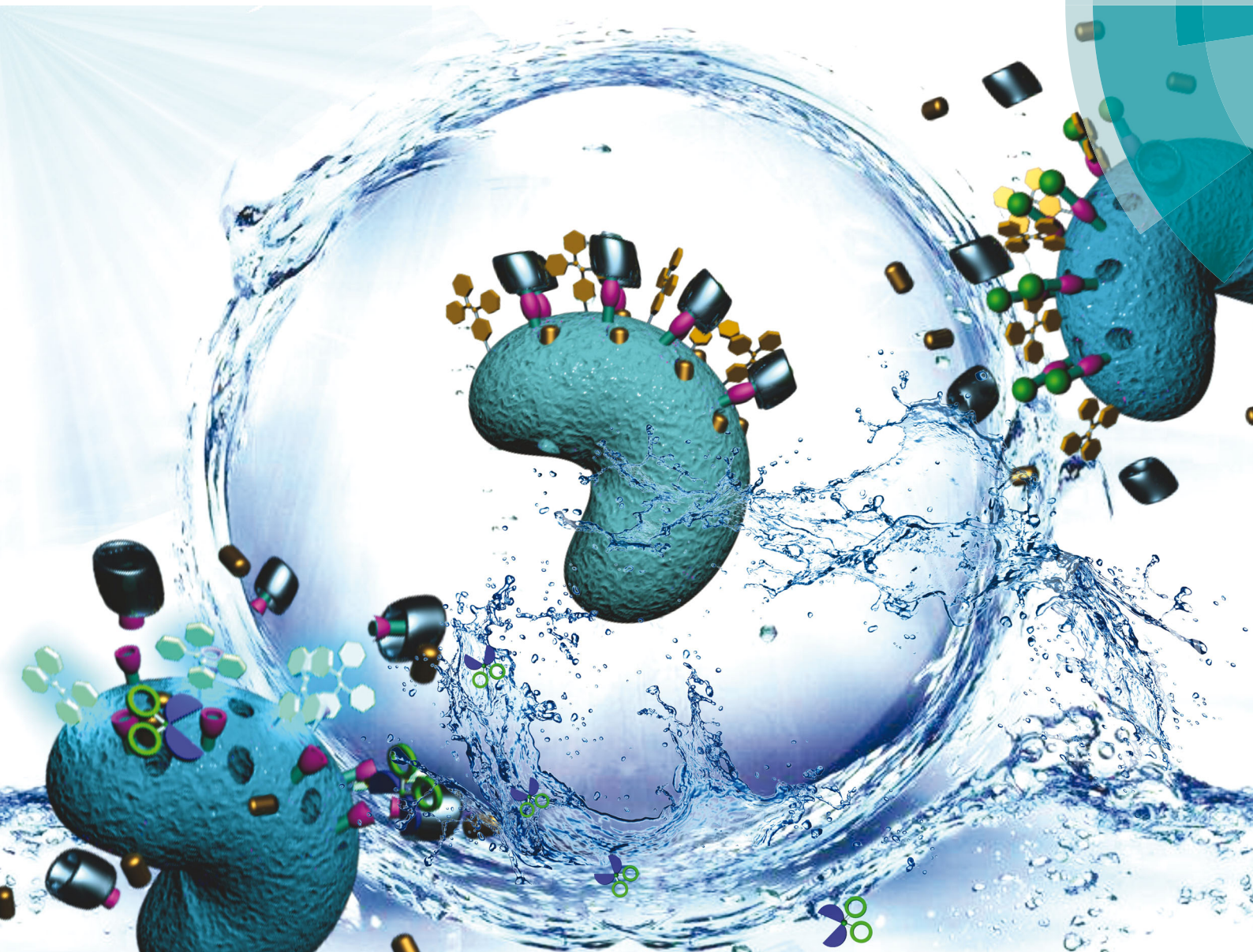


# ChemComm

Chemical Communications

rsc.li/chemcomm



ISSN 1359-7345



ROYAL SOCIETY  
OF CHEMISTRY

Celebrating  
IYPT 2019

**COMMUNICATION**

Lei Fang, Ying-Wei Yang *et al.*

Mesoporous silica nanobeans dual-functionalized with AlEgens and leaning pillar[6]arene-based supramolecular switches for imaging and stimuli-responsive drug release

Cite this: *Chem. Commun.*, 2019, 55, 14099Received 12th September 2019,  
Accepted 9th October 2019

DOI: 10.1039/c9cc07115f

rsc.li/chemcomm

# Mesoporous silica nanobeans dual-functionalized with AIEgens and leaning pillar[6]arene-based supramolecular switches for imaging and stimuli-responsive drug release†

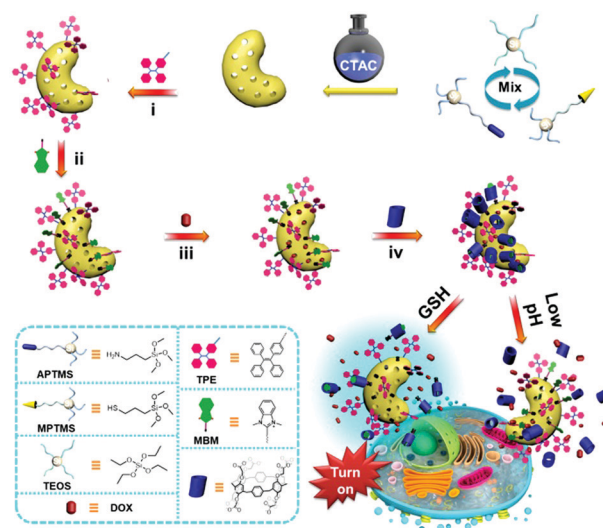
 Xiangshuai Li,<sup>‡,ab</sup> Junyou Han,<sup>‡,b</sup> Jianchun Qin,<sup>‡,b</sup> Ming Sun,<sup>c</sup> Jiarui Wu,<sup>id a</sup>  
 Liancheng Lei,<sup>c</sup> Jing Li,<sup>a</sup> Lei Fang<sup>id \*d</sup> and Ying-Wei Yang<sup>id \*a</sup>

**A bean-shaped and dual-functionalized organic–inorganic hybrid supramolecular system with a GSH-dependent turn-on fluorescence enhancement property and stimuli-responsive drug delivery function endowed with leaning towerarene-based switches has been constructed for simultaneous tumor inhibition and imaging.**

Significant advances in the fabrication of porous solids with ordered structures and new morphologies have promoted and broadened the application of these functional materials in the past couple of decades.<sup>1–3</sup> Recent development in the control of the particle shapes of silica materials, anisotropic structures in particular, has boosted intriguing applications in catalysis, energy storage, drug delivery, and bioimaging.<sup>4,5</sup> As one of the most popular drug delivery platforms, mesoporous silica nanoparticles (MSNs) attracted tremendous attention due to their large loading capacity, good biocompatibility, well-ordered pore channels, and ease of functionalization.<sup>6,7</sup> Thus, many researchers have devoted themselves to mediating the morphology, surface functionalities, loading capacity, and particle size of MSNs for biomedical applications.<sup>8–10</sup> To date, MSNs with interesting morphologies, including sphere,<sup>11</sup> rod,<sup>12</sup> bowl,<sup>13</sup> pod,<sup>14</sup> and star<sup>15</sup> shapes, and unique functions have been prepared and used in building drug delivery systems. However, usage of the reported MSNs was greatly restricted because most of them only have unique functional groups on their surfaces that could only perform limited functions.<sup>16,17</sup> It is imperative to synthesize new shaped MSNs with multiple functions and enhanced properties to broaden and strengthen the applications of mesoporous silica

frameworks and thus satisfy the growing needs. To inhibit and cure tumours more effectively, diagnosis and tracing cell uptake mechanisms of nanomedicine are critical. The AIE features permit strong emission of fluorophores even in highly aggregated states that will overcome the ACQ problems and enable the development of fluorescence “turn-on” probes for bio-imaging.<sup>18,19</sup>

Herein, we construct a bean-shaped mechanized MSN delivery system, that is, a dual-functionalized mesoporous silica nanobean, denoted as DF-MSNB, which possesses large drug loading capacity and the capability of simultaneously indicating tumour sites and eliminating tumour cells (Scheme 1). Briefly, nanobean shaped MSNs with two different functional groups (–NH<sub>2</sub> and –SH) have been prepared *via* a one-pot co-condensation method. Then a TPE derivative was conjugated upon reaction with –NH<sub>2</sub> on the MSNB to provide potential imaging function, and



**Scheme 1** Schematic illustration of MSNB preparation for application in GSH/pH dual-stimuli responsive tumour theranostics with simultaneous cell imaging. The construction of the DOX@DF-MSNB system has four steps: (i) connection of TPE, (ii) conjunction of MBM, (iii) loading of DOX, and (iv) capping with AWLP6.

<sup>a</sup> College of Chemistry, Jilin University, 2699 Qianjin Street, Changchun 130012, China. E-mail: ywyang@jlu.edu.cn

<sup>b</sup> College of Plant Science, Jilin University, 5333 Xi'an Street, Changchun 130062, China

<sup>c</sup> College of Veterinary Medicine, Jilin University, 5333 Xi'an Street, Changchun 130062, China

<sup>d</sup> Department of Chemistry, Texas A&M University 3255 TAMU, College Station, TX 77843-3255, USA. E-mail: fang@chem.tamu.edu

† Electronic supplementary information (ESI) available. See DOI: 10.1039/c9cc07115f

‡ These authors contributed equally to this work.

1,3-dimethyl-benzimidazolium (MBM) stalks were installed *via* disulfide bond formation. Taking advantage of the flexible structure, superior cavity adaptability, and guest selectivity of leaning towerarenes we recently discovered,<sup>20</sup> we further synthesized a water-soluble version of leaning pillar[6]arene (AWLP6)<sup>21</sup> to thread onto the MBM stalks on the MSNB, leading to the formation of MBM $\subset$ AWLP6 pseudorotaxane-based supramolecular nanovalves to prevent premature drug leakage from the pores and regulate the on-command release of drugs. Notably, MBM can efficiently quench TPE fluorescence (OFF) *via* donor-acceptor type electron transfer (ET), resulting in a relatively weaker system emission.<sup>22</sup> Upon encountering GSH, disulfide bond-connected MBM on the surface can be cut off, and as a result, system fluorescence can be greatly enhanced (ON), enabling the DF-MSNB to probe tumour cell sites of a high level of GSH. Benefiting from the supramolecular nanovalves based on MBM $\subset$ AWLP6 and dynamic disulfide bonds, the DF-MSNB system can regulate drug release in response to certain conditions such as a tumour microenvironment (TME) that is acidic and contains high concentration of GSH.<sup>23,24</sup> Experimental results suggest that the DOX-loaded DF-MSNB (DOX@DF-MSNB) could kill tumour cells and simultaneously serve as a “turn-on” probe for tumour cell imaging.

The synthetic strategy for the MSNB follows a specific addition order change of precursors, addition order of organo-silanes is critical for nanobean formation. Deprotonated MPTMS under high pH conditions will hinder the bending of negatively charged silica-surfactant cylinder micelle walls due to the charge repulsion between the deprotonated MPTMS and the silica-surfactant cylinder micelle walls, thus resulting in the vertical growth. However, when the silica source is TEOS and/or APTMS, the growth of the silica-surfactant cylinder micelle walls will not be affected and they will be gradually curved to be sphere-shaped (Fig. S1, ESI $\dagger$ ). In these cases, TEOS, MPTMS, and APTMS were mixed together to be a homogenous silica source solution according to the order: 1st TEOS, 2nd MPTMS, and 3rd APTMS (the adding interval is *ca.* 30 seconds). After a co-condensation procedure, the MSN morphology observed using a scanning electron microscope (SEM) and a transmission electron microscope (TEM) can be concisely controlled to be bean-shape (Fig. 1A and B). The existence of APTMS relieves charge repulsion of the deprotonated MPTMS and silica-surfactant cylinder micelle walls, leading to the formation of a partially curved bean-like MSNB.

The MSNB exhibits highly ordered 2D meso-channels according to the result of sharp 100 crystal planes in its X-ray diffraction (XRD) pattern (Fig. 1C). N<sub>2</sub> adsorption-desorption analysis of the MSNB illustrates its large surface area of 872.0 m<sup>2</sup> g<sup>-1</sup>, and pore volume of 0.54 mL g<sup>-1</sup>, and its pore size is 2.2 nm (Fig. 1D). Compared with spherical and rod shaped MSNs (MSNS and MSNR), the newly obtained MSNB shows more regular channels and large surface areas based on the results of XRD patterns and BET analysis (Fig. S2, ESI $\dagger$ ). Meanwhile, although the surface areas of the MSNR and MSNB are comparable, the relatively large size of the MSNR greatly hinders the *in vivo* application.<sup>25</sup> Notably, possessing two different reactive groups (-NH<sub>2</sub> and -SH), the MSNB was permitted to be

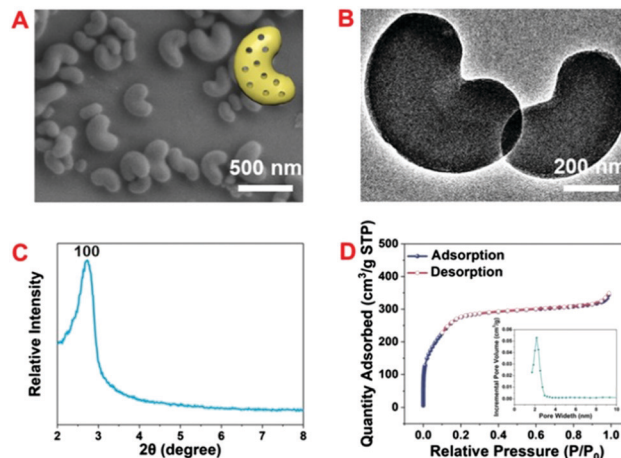


Fig. 1 (A) SEM image, (B) TEM image, (C) XRD pattern, and (D) N<sub>2</sub> adsorption-desorption isotherms and pore size distribution of the MSNB.

modified with more fantastic functionalities, endowing this nano-platform with more potential applications. Two main functionalities, *i.e.*, TPE as a widely used AIEgen that can provide monitoring function, and MBM $\subset$ AWLP6-based supramolecular nanovalves capable of reducing cargo leakage and regulating the release of drugs, have been introduced into the MSNB delivery system *via* covalent bonds (Fig. S3–S5, ESI $\dagger$ ). The TPE-functionalized MSNB (MSNB-TPE) showed strong fluorescence and a quantum yield of 5.08% due to the restriction of the intramolecular motion of TPE resulting from the covalent bonding between TPE and the MSNB (Fig. S6 and S7, ESI $\dagger$ ). A model guest, 1,2,3-trimethylbenzimidazolium iodide (MBM-CH<sub>3</sub>), was prepared to bind with AWLP6 to prove the host-guest interaction of MBM and AWLP6. From <sup>1</sup>H NMR titration, the host-guest binding constant ( $K_a$ ) was calculated to be  $(2.7 \pm 0.5) \times 10^3 \text{ M}^{-1}$  (Fig. S8 and S9, ESI $\dagger$ ). Detailed synthetic information is provided in the ESI $\dagger$  (Fig. S10–S17).

The DF-MSNB system possesses good GSH-induced fluorescence enhancement property (Fig. 2A), and its TEM image (Fig. 2B) also proved its bean-shaped morphology. Upon increasing the GSH concentration, the fluorescence intensity of the DF-MSNB obviously increased (Fig. 2C and Fig. S18, ESI $\dagger$ ). To use the fluorescent drug delivery system, the stimuli-responsive optical properties of the DF-MSNB were examined under TME mimic conditions (pH = 5.0 and [GSH] = 20 mM). Obviously, the DF-MSNB also exhibited GSH-dependent fluorescence enhancement (Fig. 2D). The fluorescence behavior of MSNB-TPE-MBM against GSH follows a linear relationship, and  $K_{SV}$  was calculated to be *ca.*  $-1.3 \times 10^2$  (Fig. S19, ESI $\dagger$ ). In the case of MBM, upon excitation, electrons can easily transfer from the conduction band (CB) of TPE to the LUMO of MBM, leading to fluorescence quenching due to the ET process (Fig. 2A).<sup>22</sup> Cyclic voltammetry (CV) was performed to further certify the ET identity. As in Fig. S20 (ESI $\dagger$ ), since a disulfide bond-linked electron-deficient molecule MBM or MBM $\subset$ AWLP6 can be cut off by GSH, upon treatment with 20 mM GSH, MSNB-TPE-MBM and DF-MSNB all exhibited a decreased reduction potential from  $-0.83$  to  $-0.99$  V and  $-0.84$  to  $-0.99$  V, respectively. The less negative reduction potentials indicated that MBM has a high reduction potential and it is easier

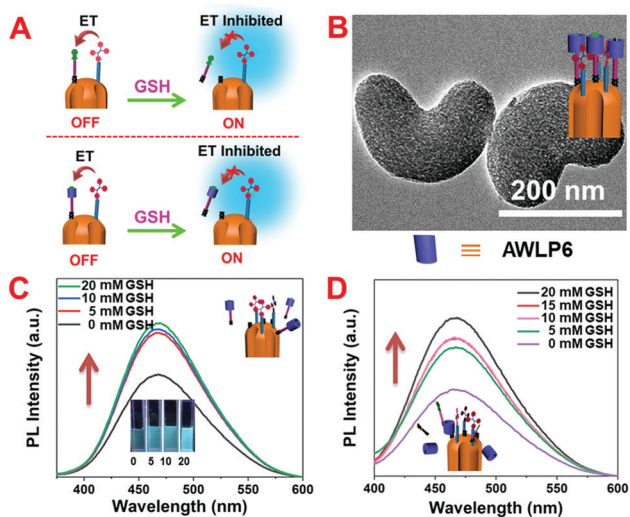


Fig. 2 (A) Schematic illustration of the GSH-induced fluorescence enhancement phenomenon of MSNB-TPE-MBM and DF-MSN. TEM image of (B) DF-MSN. GSH-dependent fluorescence enhancement of the DF-MSN in (C) deionized water and (D) TME mimic conditions ( $0.25 \text{ mg mL}^{-1}$ ;  $\lambda_{\text{ex}} = 317 \text{ nm}$ ,  $\lambda_{\text{em}} = 475 \text{ nm}$ , slit widths: ex = 5 nm, em = 3 nm).

for MBM to accept electrons from the photo-excited state of TPE, serving as an acceptor in the system.<sup>22</sup>

On the other hand, the fluorescence lifetime of the DF-MSN was increased from 2.6 ns to 3.2 ns after treatment with 20 mM GSH, which is ascribed to the inhibition of ET resulting from the removal of MBM entities (Fig. S21, ESI<sup>†</sup>). If the positively charged MBM unit of the system was replaced with a similar neutral molecule (BM), the fluorescence intensity of MSNB-TPE-BM becomes much higher than that of MSNB-TPE-MBM at the same concentration (Fig. S22A, ESI<sup>†</sup>), indicating that no fluorescence quenching occurs in the absence of MBM. After that, TPE-Br was mixed with a model electron-withdrawing molecule (MBM-CH<sub>3</sub>) in water to test fluorescence changes. As in Fig. S22B (ESI<sup>†</sup>), with a constant concentration of TPE-Br, and upon increasing the amount of MBM-CH<sub>3</sub>, the fluorescence of TPE-Br solution gradually decreased.

The DOX loading capacity of the MSNB was calculated to be  $222 \text{ mg g}^{-1}$  (DOX/DOX@DF-MSN, m/m) which is 2–3 times higher than those of most traditional MSNs, and the details of the *in vitro* release experiment are provided in the ESI<sup>†</sup> (Fig. S23).<sup>26,27</sup> Since the MBM entities were covalently connected to the MSNB through disulfide bonds, MBM-AWLP6 pseudorotaxanes would be cleaved off by GSH to release DOX. The host-guest complexation of the negatively charged AWLP6 with the positively charged MBM stalks mainly relies on electrostatic interactions. However, under acidic conditions, the carboxylate (COO<sup>-</sup>) groups of AWLP6 will turn into COOH groups, losing the electrostatic attractions with MBM thus leading to nanovalue opening and drug release (Fig. 3A).

As in Fig. 3B, without any stimuli, a negligible amount of DOX ( $5.3 \pm 0.9\%$ ) was released from the DOX@DF-MSN after being dispersed in deionized water for 22 hours. As expected, with an increasing concentration of GSH, the DOX release rate increases gradually. When the DOX@DF-MSN was incubated

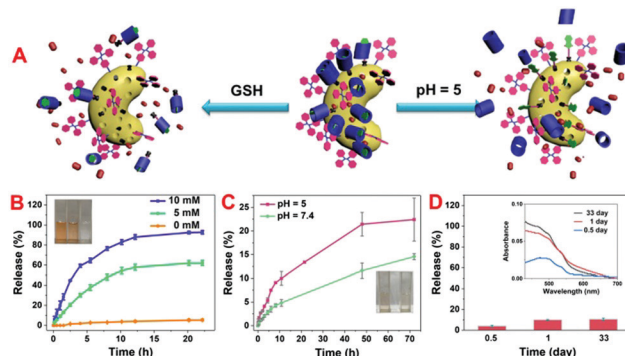


Fig. 3 (A) Schematic presentation of drug release behaviour of the DOX@DF-MSN by GSH and/or under acidic conditions. Time-dependent DOX release profiles from 0.5 mg of the DOX@DF-MSN platform (B) at different concentrations of GSH (the inset shows the digital photos of final solutions with different concentrations of GSH for 22 h: from left to right, 10 mM, 5 mM and 0 mM, respectively), (C) in the PBS solutions of different pH values (the inset shows the digital photos taken after the DOX@DF-MSN was placed in PBS solutions of different pH for 72 h: from left to right, pH 5 and 7.4). (D) Premature release of the DOX@DF-MSN in deionized water for different periods of time (the inset shows the absorbance spectra of the released DOX after placing the material in deionized water for 0.5, 1 and 33 days, respectively).

in solutions containing 5 mM or 10 mM of GSH for 22 hours, the cumulative release percentage of DOX reached  $63.0 \pm 2.5\%$  or  $92.7 \pm 1.8\%$ , respectively, which was also confirmed by the solution color changes. Meanwhile, the DOX@DF-MSN was incubated in PBS solution of pH 5 and 7.4, respectively, to investigate its pH-responsive ability. Under neutral conditions, drugs were kept tightly in the pores of the MSNB, showing negligible release, however, the release rate and amount of DOX greatly increased in the acidic solution of pH 5 (Fig. 3C). When the DOX@DF-MSN was placed in water without the activation of any stimulus, only a small amount of DOX ( $4.0 \pm 0.7\%$  and  $9.9 \pm 0.4\%$ ) was released after standing for 12 hours and 3 days, respectively. Notably, even for prolonged monitoring of drug leakage from the DOX@DF-MSN for over a month (33 days herein), only  $10.5 \pm 1.2\%$  of drug was released, indicating the excellent drug storage ability and high stability of this DF-MSN system (Fig. 3D).

The cytotoxicity of the DF-MSN was tested using a MTT assay on a human normal hepatic cell line (L02). From Fig. 4A, incubation of even  $200 \mu\text{g mL}^{-1}$  of the DF-MSN with L02 cells for 24 hours showed a negligible effect on the cells, indicating the non-cytotoxicity of the DF-MSN. After incubation with a high concentration of DF-MSN of up to  $200 \mu\text{g mL}^{-1}$  for 24 h, the DF-MSN without DOX has a negligible effect on HepG2 tumour cells (Fig. 4B). From Fig. 4C and D, free DOX and DOX@DF-MSN show an obvious effect in tumour cell killing, where the viability of the HepG2 cells was decreased obviously with increasing concentrations of DOX and DOX@DF-MSN, respectively. That is to say, the main active anticancer component of the DOX@DF-MSN is DOX with a loading ratio of 22.2% (m/m). Finally, the intracellular tumour monitoring function was tested. As in Fig. 4E, upon increasing the incubation time with the DF-MSN ( $100 \mu\text{g mL}^{-1}$ ), blue fluorescence

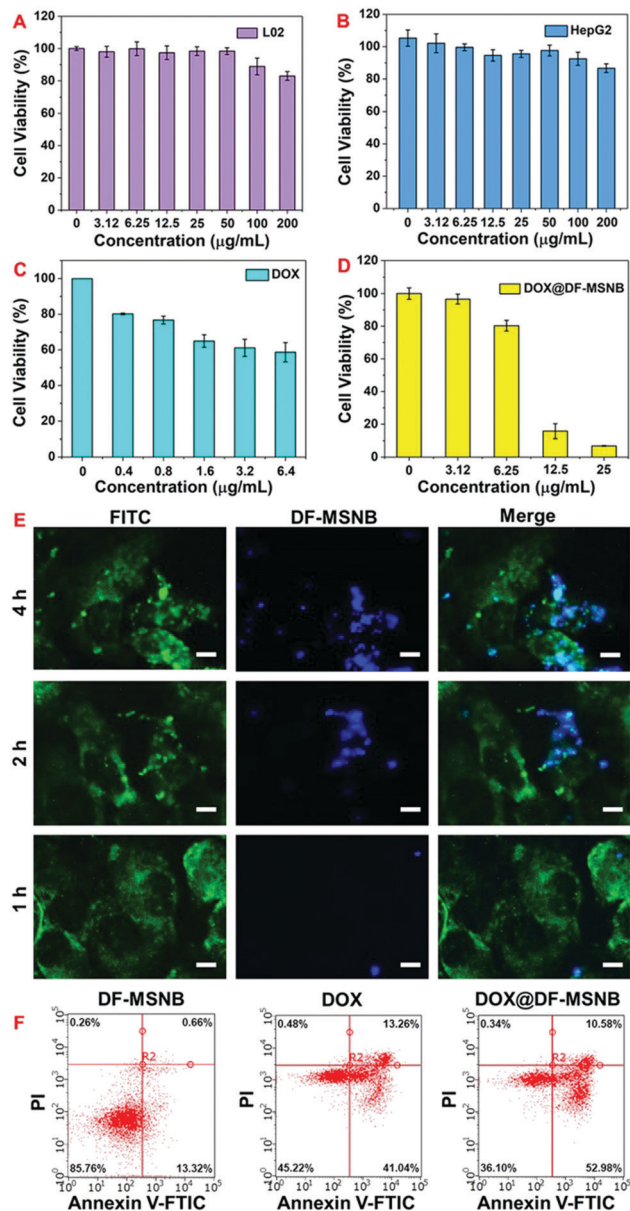


Fig. 4 Cytotoxicity of the DF-MSNB on (A) L02 and (B) HepG2 cells. Inhibition effect of (C) DOX and (D) DOX@DF-MSNB on HepG2 cells. (E) Fluorescence microscopy images of HepG2 cells after treatment with 100  $\mu\text{g mL}^{-1}$  DF-MSNB for 1 h, 2 h, and 4 h separately, scale bar = 40  $\mu\text{m}$ . (F) Flow cytometric analysis of HepG2 cells incubated with the DF-MSNB (100  $\mu\text{g mL}^{-1}$ ), DOX (6  $\mu\text{g mL}^{-1}$ ) and DOX@DF-MSNB (30  $\mu\text{g mL}^{-1}$ ) for 24 h.

in the HepG2 cells became stronger and stronger. Therefore, the DF-MSNB system was proven to be capable of imaging tumour cells. Cell apoptosis studies were further performed by the Annexin V-FITC/PI dual-staining method. The pure material DF-MSNB shows nearly no influence on HepG2 cells while the apoptosis rate of 54.3% and 63.56% of HepG2 cells induced by DOX and DOX@DF-MSNB strongly indicated their efficient therapeutic effects on tumour cells (Fig. 4F).

In conclusion, a mechanized bean-shaped DF-MSNB system with large loading capacity and nearly zero premature release of drugs was constructed, which showed not only GSH and pH dual-responsive drug release but also GSH-dependent “turn-on” fluorescence enhancement suitable for cell imaging. Proof-of-concept intracellular studies demonstrated that the DOX@DF-MSNB system could be efficiently used for tumour inhibition, and the tumour cells were able to emit blue fluorescence upon interaction with the DF-MSNB system.

This work was supported by the National Natural Science Foundation of China (51673084 and 21871108).

## Conflicts of interest

There are no conflicts to declare.

## Notes and references

- M. E. Davis, *Nature*, 2002, **417**, 813.
- Y. Lu, Y. Yang, A. Sellinger, M. Lu, J. Huang, H. Fan, R. Haddad, G. Lopez, A. R. Burns, D. Y. Sasaki, J. Shelnett and C. J. Brinker, *Nature*, 2001, **410**, 913.
- D. Zhao, J. Feng, Q. Huo, N. Melosh, G. H. Fredrickson, B. F. Chmelka and G. D. Stucky, *Science*, 1998, **279**, 548.
- S. Che, A. E. Garcia-Bennett, T. Yokoi, K. Sakamoto, H. Kunieda, O. Terasaki and T. Tatsumi, *Nat. Mater.*, 2003, **2**, 801.
- Q. Xi, M. A. Alibakhshi, S. Jiao, Z. Xu, M. Hempel, J. Kong, H. G. Park and C. Duan, *Nat. Nanotechnol.*, 2018, **13**, 238.
- N. K. Mal, M. Fujiwara and Y. Tanaka, *Nature*, 2003, **421**, 350.
- S. Mura, J. Nicolas and P. Couvreur, *Nat. Mater.*, 2013, **12**, 991.
- Y. Zhao, B. G. Trewyn, I. I. Slowing and V. S.-Y. Lin, *J. Am. Chem. Soc.*, 2009, **131**, 8398.
- H.-Y. Chiu, D. Gößl, L. Haddick, H. Engelke and T. Bein, *Chem. Mater.*, 2018, **30**, 644.
- H. Djojoputro, X. F. Zhou, S. Z. Qiao, L. Z. Wang, C. Z. Yu and G. Q. Lu, *J. Am. Chem. Soc.*, 2006, **128**, 6320.
- R. Jin, Z. Liu, Y. Bai, Y. Zhou, J. J. Gooding and X. Chen, *Adv. Funct. Mater.*, 2018, **28**, 1801961.
- Y. You, L. He, B. Ma and T. Chen, *Adv. Funct. Mater.*, 2017, **27**, 1703313.
- H. Sun, D. Liu and J. Du, *Chem. Sci.*, 2019, **10**, 657.
- S. Yang, X. Zhou, P. Yuan, M. Yu, S. Xie, J. Zou, G. Q. Lu and C. Yu, *Angew. Chem., Int. Ed.*, 2007, **46**, 8579.
- Y. Wang, N. Zhao and F.-J. Xu, *Adv. Funct. Mater.*, 2017, **27**, 1700256.
- S. Giri, B. G. Trewyn, M. P. Stellmaker and V. S. Y. Lin, *Angew. Chem., Int. Ed.*, 2005, **44**, 5038.
- R. A. Perez, R. K. Singh, T. H. Kim and H. W. Kim, *Mater. Horiz.*, 2017, **4**, 772.
- J. Mei, Y. Hong, J. W. Lam, A. Qin, Y. Tang and B. Z. Tang, *Adv. Mater.*, 2014, **26**, 5429.
- X. Wei, M. J. Zhu, Z. Cheng, M. Lee, H. Yan, C. Lu and J. J. Xu, *Angew. Chem., Int. Ed.*, 2019, **58**, 3162.
- J.-R. Wu, A. Mu, B. Li, C.-Y. Wang, L. Fang and Y.-W. Yang, *Angew. Chem., Int. Ed.*, 2018, **57**, 9853.
- X. Wang, J.-R. Wu, F. Liang and Y.-W. Yang, *Org. Lett.*, 2019, **21**, 5215.
- S. Pramanik, C. Zheng, X. Zhang, T. J. Emge and J. Li, *J. Am. Chem. Soc.*, 2011, **133**, 4153.
- M.-X. Wu and Y.-W. Yang, *Adv. Mater.*, 2017, **29**, 1606134.
- Y.-W. Yang, Y.-L. Sun and N. Song, *Acc. Chem. Res.*, 2014, **47**, 1950.
- Y. Liu, P. Bhattacharai, Z. Dai and X. Chen, *Chem. Soc. Rev.*, 2019, **48**, 2053.
- Q.-L. Li, D. Wang, Y. Cui, Z. Fan, L. Ren, D. Li and J. Yu, *ACS Appl. Mater. Interfaces*, 2018, **10**, 12155.
- X. Li, J. Han, X. Wang, Y. Zhang, C. Jia, J. Qin, C. Wang, J.-R. Wu, W. Fang and Y.-W. Yang, *Mater. Chem. Front.*, 2019, **3**, 103.